

Identification of a superagonist variant of the immunodominant Yellow fever virus epitope NS4b₂₁₄₋₂₂₂ by combinatorial peptide library screening

Amandine Bovay^a, Vincent Zoete^{b,c}, Pierre J. Rizkallah^d, Konrad Beck^e, Philippe Delbreil^a, Daniel E. Speiser^a, David K. Cole^d, Silvia A. Fuertes Marraco^{a,*}

^a Department of Oncology, Lausanne University Hospital (CHUV), Lausanne, Switzerland

^b Department of oncology CHUV-UNIL, Ludwig Institute for Cancer Research, Epalinges, Switzerland

^c SIB Swiss Institute of Bioinformatics, Molecular Modeling Group, Lausanne, Switzerland

^d Division of Infection and Immunity and Systems Immunity Research Institute, Cardiff University School of Medicine, Heath Park, Cardiff, United Kingdom

^e Cardiff University School of Dentistry, Heath Park, Cardiff, United Kingdom

ARTICLE INFO

Keywords:

Altered peptide ligand
Peptide rigidity
Antigen sensitivity
CD8 T cells
Yellow fever virus

ABSTRACT

The CD8 T cell response to the HLA-A2-restricted epitope LLWNGPMAV (LLW) of the non-structural protein 1b of Yellow Fever Virus (YFV) is remarkably immunodominant, highly prevalent and powerful in YFV-vaccinated humans. Here we used a combinatorial peptide library screening in the context of an A2/LLW-specific CD8 T cell clone to identify a superagonist that features a methionine to isoleucine substitution at position 7. Based on *in silico* modeling, the functional enhancement of this LLW-7I mutation was associated with alterations in the structural dynamics of the peptide in the major histocompatibility complex (pMHC) binding with the T cell receptor (TCR). While the TCR off-rate of LLW-7I pMHC is comparable to the wild type peptide, the rigidity of the 7I peptide seems to confer less entropy loss upon TCR binding. This LLW-7I superagonist is an example of improved functionality in human CD8 T cells associated with optimized ligand rigidity for TCR binding and not with changes in TCR:pMHC off-rate kinetics.

1. Introduction

T cells respond to proteic antigens in the form of short peptides, usually between 8 and about 20 amino acids in length. Cytotoxic CD8 T cells recognize peptides derived from proteins processed by the endogenous pathway and presented on Major Histocompatibility Complex (MHC) Class I molecules for interaction with cognate T cell receptors (TCRs). Upon encounter with their cognate peptide-MHC (pMHC) complex, TCR triggering activates a signaling cascade leading to the proliferation and initiation of effector functions by T cells.

Several studies suggest that a potent T cell response is related to a lower dissociation constant (K_D) and/or a longer monomeric dissociation constant rate (k_{off}) (Gannon et al., 2015; Hebeisen et al., 2015; Holler et al., 2001; La Gruta et al., 2006; Matsui et al., 1994; Tian et al., 2007). A recent report on self/tumor and virus-specific CD8 T cell clones showed that k_{off} values offer a better prediction of the CD8 T cell potency (Allard et al., 2017). However, TCRs often weakly interact with pMHC complexes (1–100 μ M) and with fast dissociation kinetics ($k_{off} > 0.01$) (Cole et al., 2007; Davis et al., 1998; Stone and Kranz, 2013). As low affinity T cells participate in the anti-tumor immune

response, the TCR-pMHC binding parameters are of particular importance in the context of immunotherapies of cancer. Several clinical trials conducted on cancer patients examined the impact of adoptively transferred T cells expressing affinity-improved TCRs on clinical outcome. They concluded that optimal T cell function occurs at intermediate TCR:pMHC binding strength, highlighting a TCR affinity threshold for maximal T cell responses (Dutoit et al., 2001; Gannon et al., 2015; Speiser et al., 2008; Tan et al., 2015; Zhong et al., 2013).

In the present study, we explore the functionality of a TCR identified in a CD8 T cell clone (YF5048) isolated from a healthy volunteer vaccinated with the live-attenuated Yellow Fever virus vaccine YF-17D. YF5048 is specific for the immunodominant HLA-A*0201-restricted epitope LLWNGPMAV (NS4b 214–222; hereafter A2/LLW). Upon vaccination with YF-17D, the CD8 T cell response to this A2/LLW epitope *in vivo* is remarkably immunodominant: it is highly prevalent (the majority of HLA-A*02 individuals will raise a response) and predominates the specificity of the response; this epitope alone can represent in the range of 10 % of the CD8 T cell response (Akondy et al., 2009; Blom et al., 2013; Bovay et al., 2017; Marraco et al., 2015; de Melo et al., 2013). Previously, we reported the crystal structure of the

* Corresponding author.

E-mail address: silvia.fuertes@chuv.ch (S.A. Fuertes Marraco).

LLW peptide in complex with HLA-A*02 and performed *in silico* modeling of TCR binding based on the TCR sequence of clone YF5048 (Bovay et al., 2017). Here we describe an altered peptide of the LLW nonamer that induces increased functionality in the YF5048 clone and investigate the particular structural and dynamic properties that are associated with such increased antigen sensitivity.

2. Material and methods

2.1. Sizing scan

The following mixtures were used to define the peptide length preference of individual TCRs: X⁸, X⁹, X¹⁰, X¹¹, X¹², and X¹³ (where X is any of the 19 L-amino acids excluding cysteine; Pepscan Presto) (Ekeruche-Makinde et al., 2013). The YF5048 clones were washed and rested overnight in R5 medium (RPMI 1640 supplemented with 100 units/mL penicillin, 100 µg/mL streptomycin, 2 mM l-glutamine, and 5% heat-inactivated fetal calf serum (all Invitrogen)). In U-bottom 96-well plates, 6×10^4 target cells were incubated with sizing scan mixtures at 1 mM in duplicate for 2 h at 37 °C. After peptide pulsing, 3×10^4 YF5048 clone were added and the assay was incubated overnight at 37 °C. Subsequently, the supernatant was harvested and assayed for MIP-1β by ELISA according to the manufacturer's instructions (R&D Systems).

2.2. ⁵¹Chromium release assay

The ⁵¹Chromium release assay was performed as described previously (Bovay et al., 2017). The HLA-A*02⁺ human mutant cell line CEMx721.T2 (American Type Culture Collection) was used as target by labeling with ⁵¹Cr for 1 h at 37 °C, followed by extensive washing. Target cell killing was assessed by chromium release in the supernatant upon co-culture with the YF5048 clone (effector cells) at the Effector: Target ratio of 10:1 for 4 h at 37 °C in V-bottom microwells, in the presence of serial dilutions of the peptides, measured using a gamma counter and calculated as:

$$\% \text{ specific lysis} = 100 \times \frac{(\text{experimental} - \text{spontaneous release})}{(\text{total} - \text{spontaneous release})}$$

2.3. Intracellular cytokine staining assay

The staining was performed as described previously (Bovay et al., 2017). The YF5048 clone was stimulated with peptide-loaded T2 cells at the E:T cell ratio of 1:2 for 4 h at 37 °C in the presence of Brefeldin-A (Sigma-Aldrich) and anti-CD107a-PE antibody (BD Biosciences). Then, cells were stained with anti-CD8-APC-AF750 antibody (Beckman Coulter) at 4 °C for 30 min. After washing in PBS, cells were incubated with eFluor 455UV Fixable Viability Dye (eBioscience) at 4 °C for 30 min, and fixed with 0.36 % formaldehyde at 4 °C overnight. Cells were washed and stained intracellularly with anti-IFNγ-PC7, anti-TNFα-A700, GranzymeB-APC (BD Biosciences) and anti-IL-2-FITC antibodies (BD Biosciences) in phosphate-buffered saline (PBS) with 5 mM EDTA, 0.2 % bovine serum albumin (FACS buffer) with 0.1 % saponin for 30 min at 4 °C. Samples were acquired using an LSRII-SORP flow cytometer (BD Biosciences, five-laser configuration). The data were processed with FlowJo (Tree Star Inc., v9.5.2).

2.4. pMHC multimer staining

The T cell clone was incubated with various concentrations of the PE-labeled multimers (TC Metrix Sàrl) for 30 min in FACS buffer with 20 mM NaN₃ at 4 °C. Samples were acquired using a SORP-LSR II flow cytometer (BD Biosciences). The data were processed with FlowJo (v.9.7.6; Tree Star) and geometric mean fluorescence intensity values were plotted and analyzed using GraphPad Prism software (V6;

GraphPad). Dissociation constants K_D were calculated assuming a one-site binding model as implemented in GraphPad.

2.5. NTamer staining and dissociation kinetic measurements

Dually labeled pMHC multimers built on NTA-Ni²⁺-His-tag interactions called NTAmers (synthesized by TCMetrix Sàrl) were used for dissociation kinetic measurements (Schmidt et al., 2011, 2013). Stainings with dually PE- and Cy5-labeled A2/LLW-specific NTAmers and data analysis were done as previously described (Hebeisen et al., 2015; Schmidt et al., 2011). Briefly, staining was measured at 4 °C using a thermostat device on a SORP-LSR II flow cytometer (BD Biosciences). Following 30 s of baseline acquisition, imidazole (100 mM) was added. PE and Cy5 fluorescence were measured during the following 5 min. Data were processed using the kinetic module of the FlowJo software (v.9.7.6; Tree Star), and corrected mean fluorescence intensity values were plotted and analyzed using GraphPad Prism. An irrelevant clone (recognizing the HLA-A*0201-restricted CMV epitope pp65^{495–504}: NLVPMVATV) was used to reference the non-specific background staining. In order to overcome the potential differences of NTamer molecule's quality, the Cy5 decay values of the NTAmers specific for the mutant peptides were normalized to the PE decay value of the WT NTamer.

$$\text{Half - life} = \ln 2 / k_{\text{off}}$$

2.6. Protein expression, refolding and purification

HLA A*0201 α-chain and β2 m were expressed separately, without post-translational modification, as insoluble inclusion bodies (IBs) in competent Rosetta (DE3) *Escherichia coli* cells, using 0.5 M IPTG to induce expression as described (MacLachlan et al., 2017). Briefly, for a 1 l pMHC refold, 30 mg HLA-A*0201 α-chain was mixed with 30 mg β2 m and 4 mg peptide at 37 °C for 15 min with 10 mM DTT. This mixture was added to cold refolding buffer (50 mM Tris, pH8, 2 mM EDTA, 400 mM L-arginine, 6 mM cysteamine hydrochloride, and 4 mM cystamine). Refolded complexes were mixed at 4 °C for > 6 h. Dialysis was performed against 10 mM Tris, pH8.1, until the conductivity of the refolds was less than 2 mS/cm. Refolded proteins were filtered and purified by ion exchange using a Poros50HQTM column (GE Healthcare, Buckinghamshire, U.K.) followed by gel filtration directly into crystallization buffer (10 mM Tris pH8.1, 10 mM NaCl) or PBS (137 mM NaCl, 3 mM KCl, 8 mM Na₂HPO₄, 1 mM KH₂PO₄) using a Superdex 200 HRTM column (GE Healthcare, Buckinghamshire, U.K.). Protein quality was analyzed by Coomassie-stained SDS-PAGE under non-reducing or reducing conditions.

2.7. Thermal stability of HLA-A*0201-peptide complexes

Thermal stability of A2/peptide complexes was assessed by circular dichroism (CD) spectroscopy as described in detail in Fuller et al., 2017 (Fuller et al., 2017). Briefly, after purification by gel filtration chromatography in PBS, proteins were diluted to ca. 3.5 µM, and melting curves were recorded at 218 nm in 0.1-cm cells using an Aviv 215 spectrometer (Aviv Biomedical Inc., Lakewood, NJ). Denaturation was monitored from 4 °C up to a temperature when protein precipitation occurred using parameters resulting in a heating rate of ~36 °C/h. Melting curves were analyzed assuming a two-state native (N) to denatured (D) transition N₃ ↔ 3D with the melting temperature T_m and van't Hoff's enthalpy ΔH_{vH} at the midpoint of the transition as fitting parameters.

2.8. Crystallization, diffraction data collection, and model refinement

All protein crystals were grown at 18 °C by vapor diffusion via the "sitting drop" technique. 200 nl of each pMHC (20 mg/mL) in

crystallization buffer was added to 200 nl of reservoir solution. A2/LLW-4A crystals were grown in 0.1 M sodium cacodylate pH 6.0, 0.2 M ammonium sulphate, 25 % PEG 4000. A2/LLW-71 crystals were grown in 0.1 M Mes pH 7.0, 0.2 M ammonium sulphate, 25 % PEG 8000. A2/LLW-8H and A2/LLW-8Q crystals were grown in 0.1 M sodium cacodylate pH 6.5, 0.2 M ammonium sulphate, 20 % PEG 4000. All crystals were soaked in 30 % ethylene glycol before cryo-cooling. All crystallization screens and optimization experiments were completed using an Art-Robbins Gryphon dispensing robot (Alpha Biotech Ltd., UK). Data were collected at 100 K at the Diamond Light Source (Oxfordshire, UK) as described previously (Motozono et al., 2015). All data sets were collected at a wavelength of 0.98 Å using an ADSC Q315 CCD detector. Reflection intensities were estimated with the XIA2 package, and the data were scaled, reduced, and analyzed with the SCALA and CCP4 package. Structures were solved with molecular replacement using PHASER. A solution could be obtained with a search model taken from Protein Data Bank entry. Sequences were adjusted with COOT, and the models were refined with REFMAC5. Graphical representations were prepared with PyMOL. The reflection data and final model coordinates were deposited in the Protein Data Bank: A2/LLW-4A (6SS7), A2/LLW-71 (6SS8), A2/LLW-8H (6SS9), A2/LLW-8Q (6SSA).

2.9. Modeling the TCR-pMHC complexes

As described previously (Bovay et al., 2017), the 3D structure of the TRAV12–2/TRBV9 TCR in complex with HLA-A2 and the LLW peptide was modeled from three experimental structures: 3HG1 (Cole et al., 2009) and 4QOK (Madura et al., 2015), containing a complex between the TRAV12–2/TRBC1 TCR in complex with HLA-A2 and the ELAGI-GILTV or EAAGIGILTV peptides, respectively, and the experimental structure obtained in this study for the complex between HLA-A2 and the LLWNGPMHV, LLWNGPMQV, and LLWAGPMAV peptides. The sequence alignment between TRBV9 and TRBC1 was performed using the MUSCLE program (Edgar, 2004). The sequence identity between the variable part of the TRBV9 and TRBC1 TCR beta chains is 30 %. Based on this sequence alignment, the model was obtained using the Modeller program (Eswar et al., 2001; Šali and Blundell, 1993). 1000 models were generated by satisfaction of spatial restraints through minimization and simulated annealing, and the model with the best Modeller objective function was retained. Molecules were visualized and analyzed using UCSF Chimera (Pettersen et al., 2004).

2.10. Molecular dynamics simulations

MD simulations were performed with GROMACS (Abraham et al., 2015; Bjelkmar, 2010) version 2018.3 in periodic boundary conditions, using the all-atom CHARMM27 force field (MacKerell et al., 1998) and the TIP3P water model. The number of Na⁺ and Cl[−] ions in solution was adjusted to neutralize the system and reach the physiological concentrations of 0.154 M. Before starting the MD simulations, missing

residues and loops were modelled using the Dunbrack rotamer libraries (Dunbrack, 2002) and the Modeller program (Eswar et al., 2001). Titratable side chains were protonated so as to allow hydrogen bonds with neighbouring residues. Electrostatic interactions were calculated with the Ewald particle-mesh method (Essmann et al., 1995) with a grid spacing of 1.2 Å. A cut-off of 12 Å was applied for the real-space Coulomb and van der Waals interactions. Bonds involving hydrogen atoms were constrained using the P-LINCS algorithm (Hess et al., 2008). The system was coupled to a Parinello-Rahman barostat with a relaxation time of 1 ps. The solute and the solvent were separately coupled to two nose-hoover thermostats (Bussi et al., 2007), each with a relaxation time of 0.2 ps. A time integration step of 2 fs was used, with a temperature of 300 K and a pressure to 1 bar during the production trajectory. Initial Cartesian coordinates were taken from the experimental X-ray structures of pMHC molecules obtained in this study. Peptide mutations, M7I, A8H and A8Q were introduced using the *swapaa* command of UCSF Chimera (Pettersen et al., 2004) v 1.12 and the Dunbrack backbone-dependent rotamer library (Dunbrack, 2002). Initial structures were energy optimized, heated from 0 to 300 K in 0.4 ns, equilibrated for a further 1 ns restraining each solute non-hydrogen atom to its original position, and finally equilibrated for 2 ns without restraints before data collection. 3 MD simulations were carried out for the WT and mutated peptides to assess the reproducibility of the results. Each MD simulation had a production time of 140 ns, saving coordinates every 0.05 ns.

2.11. Statistical analysis

P-values from unpaired t-tests and data visualizations were obtained using the software Microsoft Excel 14.2.0 and GraphPad Prism 8.1.0. A p-value ≤ 0.05 was considered statistically significant.

3. Results

3.1. Identification of superagonist peptides for the A2/LLW-specific CD8 T cell clone YF5048

First, we assessed the peptide length preference of the YF5048 clone by the functional recognition of a custom-built “sizing scan” comprising random peptide libraries of different lengths (8 to 13-mer) (Ekeruche-Makinde et al., 2013). Previous data suggest that CD8 T cell clones exhibit preference for the length of the index peptide (Ekeruche-Makinde et al., 2013): as expected, we validated that the YF5048 clone exhibited a preference for the length of the index peptide (9-mer) (Fig. 1A).

In order to identify potential superagonist peptides for the YF5048 clone, we performed a combinatorial peptide library (CPL) screening (Bovay et al., 2017; Galloway et al., 2019). Only few non-index residues at positions 7 and 8 could increase the response compared to the index peptide (Bovay et al., 2017). In particular, the CPL results suggested that LLW-71 (LLWNGPIAV), LLW-8H (LLWNGPMHV) and LLW-8Q

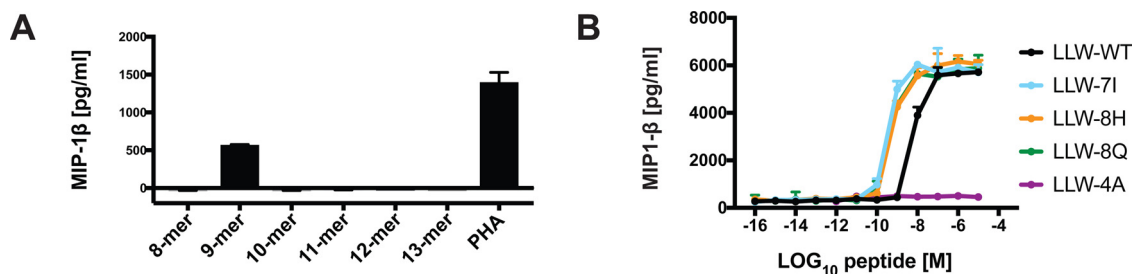


Fig. 1. Peptide recognition signature of an individual TCR derived from clone YF5048. A, Peptide length preference was determined by sizing scan comprising random peptide mixtures of different lengths. Values are expressed as the concentration of MIP-1β secreted in the supernatant measured by ELISA in duplicate (mean and SD). B, Recognition of 3 individual peptides chosen from the CPL assessed by MIP-1β activation in duplicate with graded concentrations of the peptides (mean and SD).

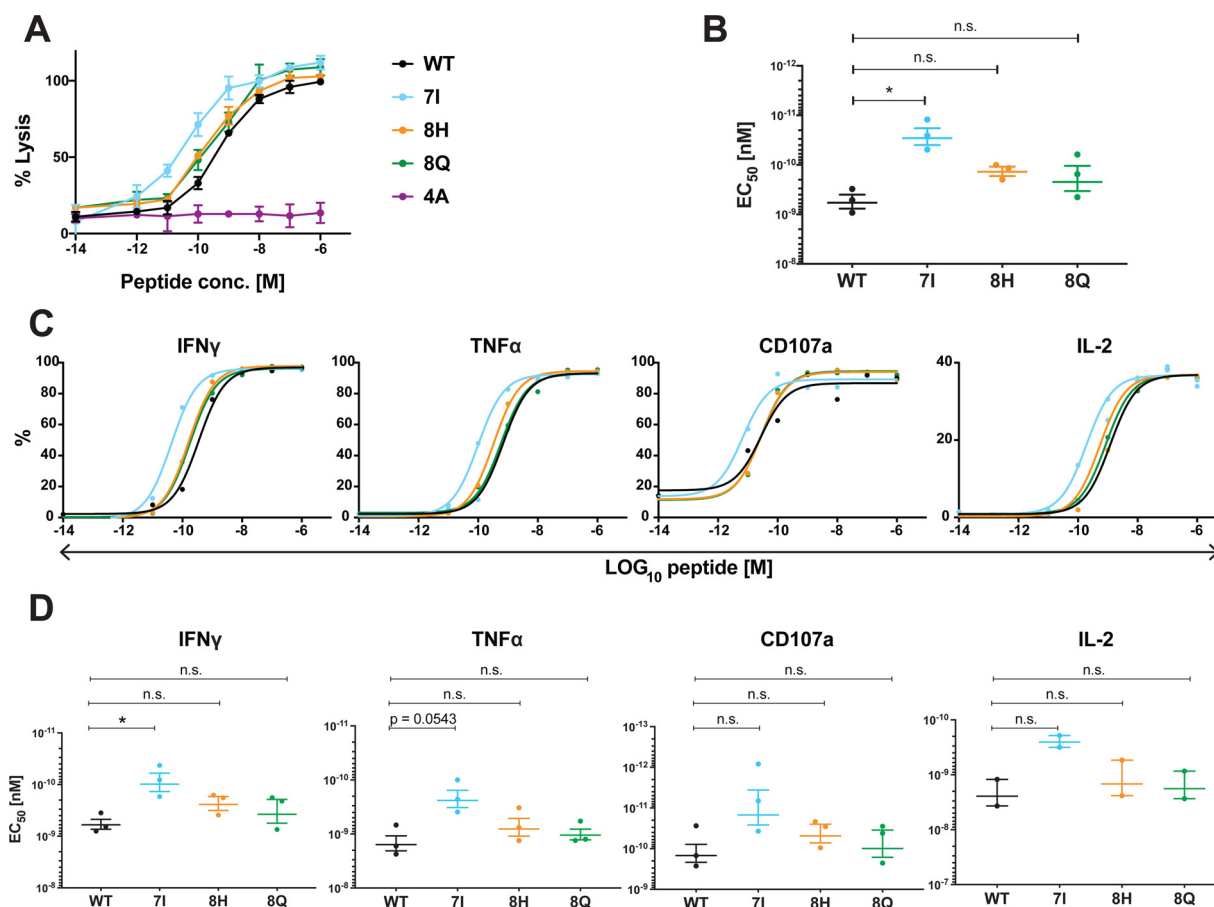


Fig. 2. Functional properties of the YF5048 clone following stimulation with mutant peptides identified by the CPL. A, Killing capacity (51-chromium release assay) with titration of the different peptides as indicated. Data are the combination of 3 independent experiments (mean and SEM). B, The EC₅₀ values of the 3 independent 51-chromium release assays shown in A (mean and SEM). C, Intracellular cytokine staining following peptides stimulation for 4 h. Data are the combination of 3 independent experiments (mean and SEM). IL-2 expression was assessed in only 2 independent experiments. D, Values of the 3 independent intracellular cytokine staining are expressed as EC₅₀ (mean and SEM). P-values from unpaired t-tests: ns = not significant, * < 0.05, ** < 0.01, *** < 0.001.

(LLWNGPMQV) are optimal peptides (Bovay et al., 2017).

Next, we tested the peptide sequences revealed by the nonamer CPL screening by stimulating with peptides individually (Fig. 1B). Indeed, the ELISA confirmed that all three mutant peptides (LLW-7I, -8H and -8Q) induced the expression of the cytokine MIP-1 β at superior levels than stimulation with LLW-WT. The LLW-4A (LLWAGPMAV) peptide served as a negative control. As shown previously (Bovay et al., 2017), residue Asn4 of the peptide made numerous favorable interactions with the TCR, including hydrogen bonds with Ser32 and Asp92 of TCR α (Fig S1). The lack of immune response to A2/LLW-4A is therefore in line with the loss of critical TCR/pMHC interactions. As previously reported, LLW-4R (LLWRGPMVA) failed to activate the TCR (Bovay et al., 2017).

We further investigated the antigen sensitivity to the mutant peptides revealed by the CPL screening. First, we assessed the killing capacity of the YF5048 clone using a chromium release assay after stimulation with these peptides (Fig. 2A and B). Upon titration, the LLW-7I peptide led to an approximately 10-fold higher antigen sensitivity than LLW-WT (Fig. 2A). This decreased EC₅₀ was significant (Fig. 2B). The response to the LLW-8H and -8Q peptides were comparable to the LLW-WT.

Second, we compared the degranulation and secretion of cytokines upon stimulation with the various peptides by flow cytometry. Stimulation with titrating amounts of the LLW-7I peptide led to an approximate 10-fold increased secretion of all measured cytokines compared to LLW-WT titration (Fig. 2C and Fig S2). The calculated EC₅₀ of the LLW-7I peptide titration was approximately 10-fold better than LLW-WT for IFN γ , TNF α and IL-2 (Fig. 2D). Similar effects were

observed for the degranulation marker CD107a (Fig. 2C and D). The peptides LLW-8H and LLW-8Q did not improve significantly the antigen sensitivity compared to LLW-WT. Also, the LLW-7I peptide induced a higher polyfunctionality at low peptide concentrations compared to the LLW-WT peptide (Fig S3).

3.2. The 7I mutation in LLW improves the TCR:pMHC dissociation constant K_D without impacting the monomeric off-rate

We hypothesized that the enhanced antigen sensitivity of the LLW-7I mutant could be a consequence of a stronger TCR:pMHC interaction. In order to characterize the interaction between the TCR and the agonist pMHC complexes, we first used fluorescently-labeled pMHC multimers at graduating concentrations and measured the fluorescence intensity upon staining of the YF5048 clone in order to calculate the dissociation constant K_D value (k_{on}/k_{off}) (Fig. 3A and B) (Wooldridge et al., 2009, 2012). The A2/LLW-7I, -8H and -8Q multimers stained the YF5048 clone with a slightly stronger intensity compared to the A2/LLW-WT multimer (Fig. 3A) and bound the TCR with a lower K_D (Fig. 3B).

Previous reports have linked higher functional avidity specifically to longer TCR:pMHC off-rates (Allard et al., 2017; Gannon et al., 2015; Hebeisen et al., 2015; Nauerth et al., 2013; Schmid, 2010). We next measured the monomeric dissociation constant rates (k_{off}) using dually labeled pMHC multimers built on NTA-Ni²⁺-His-tag interactions called NTAmers (Schmidt et al., 2011, 2013). We found that the off-rate k_{off} was highly decreased for A2/LLW-8H and -8Q compared to A2/LLW-WT

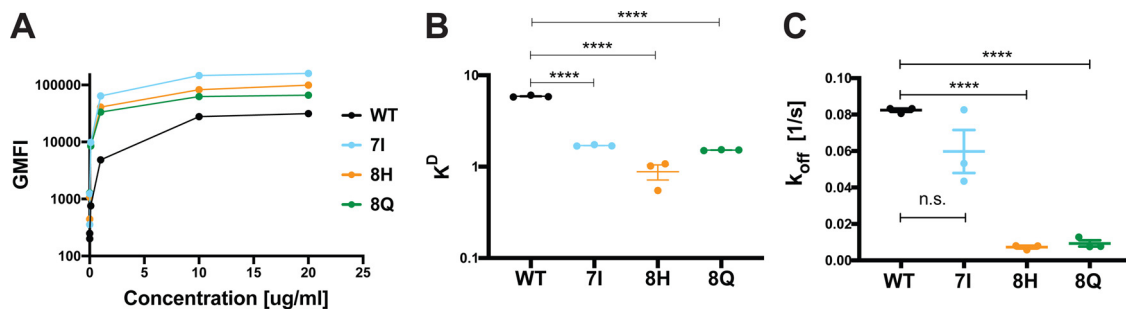


Fig. 3. TCR affinity of the YF5048 clone towards mutant peptides. A, Representative experiment comparing the geometric mean fluorescent intensities (GMFI) values of the YF5048 clone stained with the wild-type and mutant pMHC multimer at different concentrations. B, K_D values of the 3 independent multimer stainings at different concentrations were calculated assuming a one-site binding model as implemented in GraphPad. (mean and SEM). C, TCR dissociation rates (k_{off}) of the NTamer Cy5 decay normalized to PE background, calculated from the data of the 3 independent experiments (mean and SEM). P-values from unpaired t-tests: ns = not significant, * < 0.05, ** < 0.01, *** < 0.001.

(Figs. 3C, S4 and S5). Rather unexpectedly, no significant difference was observed for the k_{off} of A2/LLW-7I compared to A2/LLW-WT, such that changes in off-rates could not explain increased sensitivity of the LLW-7I peptide.

These data show that all three mutant peptides improved the K_D values compared to the WT peptide. In contrast to the A2/LLW-8H and -8Q peptides, the k_{off} value of the LLW-7I peptide was not significantly lower compared to the WT peptide.

3.3. *In silico* modeling shows no particular structural advantage in the 7I mutation of LLW, while the 8Q and 8H mutations show favorable contacts with the TCR

In order to address structural determinants of the TCR:pMHC interaction, we solved the atomic structure of the A2/LLW-7I, A2/LLW-8H and A2/LLW-8Q pMHC complexes (Table S1). We performed *in silico* modeling based on our crystal structures of the three mutant pMHC complex and the previously solved structure of the MEL5 TCR (Cole et al., 2009), which has a TCR α chain that is very close in sequence to the TCR α chain of YF5048 (Bovay et al., 2017). In these modeled structures, the LLW-8H and -8Q mutant peptides made favorable contacts with the TCR (Fig. 4A), which would explain the higher TCR avidity measured by NTamer. In contrast, the 7I substitution did not introduce additional favorable contacts with the TCR (Fig. 4B). This is in line with the lack of a particular advantage in TCR:pMHC k_{off} as measured by NTamer for the 7I mutation (Fig. 3), but still did not explain the increased functional avidity based on immunoassays upon titration with the 7I peptide (Fig. 2).

Thus, our data shows that a substitution to an isoleucine at P7 does not change the TCR k_{off} . This was further supported by our *in silico* model which shows that the 7I mutant peptide does not make more favorable contacts with the TCR compared to the WT peptide. The superior T cell function induced by the LLW-7I mutant peptide was therefore unlikely to be due to increased structural TCR:pMHC interactions.

In contrast, our data suggest that the LLW-8H and -8Q mutant peptides made favorable contacts with the TCR, supporting the significantly longer off-rates and lower K_D values compared to the WT peptide.

3.4. The 7I mutant peptide shows higher entropy loss and rigidity in complex with HLA-A*02

The enhanced T cell function observed after stimulation with the 7I mutant peptide could result from the inherent properties of the pMHC complex. To assess this, we expressed, refolded and purified HLA-A*0201 in complex with the mutant and WT peptides. To assay the peptide binding affinity to the MHC molecule, we performed circular

dichroism (CD) temperature melting experiments (Fig. 5A). The A2/LLW-7I, A2/LLW-8H and A2/LLW-8Q complexes showed a melting temperature T_m of 66.2, 65.2, 65.3 °C, respectively. Thus, the stability of the mutant complexes was not significantly different from the A2/LLW-WT complex (T_m of 66.5 °C, ΔH_{vH} of -488 kJ/mol) (Fig. 5B).

The values of transition enthalpies ΔH_{vH} were also calculated from the same experiments (Fig. 5B, bottom). The binding of the LLW-7I peptide to the MHC shows a lower, i.e. more favorable, ΔH_{vH} than the other peptides, suggesting that the entropy loss upon binding is greater and that the resultant LLW-7I mutant pMHC complex is more rigid than the LLW-WT pMHC complex.

In order to investigate pMHC rigidity further, we performed molecular dynamics (MD) simulations of the A2/LLW pMHC complex variants starting from the crystal structures of the A2/LLW-7I, A2/LLW-8H and A2/LLW-8Q complexes. The Root Mean Square Fluctuations (RMSF) of the different peptide and MHC residues were calculated. The latter constitute a measure of the vibration intensity of the residues around their average position: a residue is more flexible if its RMSF value is higher. In the A2/LLW-WT complex, the peptide residues Leu1, Asn4 and Met7, which are facing the solvent in the absence of TCR, are the most flexible residues, while the peptide residues Leu2, Trp3 and Val9, which are buried into the MHC pockets, are less flexible (Fig. 6A).

Interestingly, the isoleucine substitution at P7 of the LLW-7I mutant peptide in the pMHC complex showed a significantly decreased flexibility compared to Met7 in the LLW-WT pMHC complex (Fig. 6A).

As expected, the difference between the RMSF of the other peptide residues between the LLW-WT and -7I mutant were not significant (Fig. 6A). Also, the flexibility of Met7 in the LLW-8H and LLW-8Q mutants was similar to that of the WT peptide.

His8 and Gln8 contain more dihedral angles than the Ala8 residue in the WT system, and can be expected to display more flexibility when they face the solvent, in absence of TCR. This is indeed what was observed in the MD simulations for residues His8 and Gln8, in the MD simulations of the A2/LLW-8H and -8Q complexes, compared to Ala8 of the WT complex. However, this increase in flexibility compared to Ala8 was limited and not statistically significant (Fig. 6A). The corresponding small entropy penalty upon binding for the mutated systems was compensated by the additional interactions made between the His8 or Gln8 side chains and TCR, compared to Ala8 in the WT system as suggested by our *in silico* model (Fig. 4A and B).

The peptide substitutions could potentially modify the MHC flexibility. To control for this, the RMSF of the MHC residues were calculated from the same MD simulations (Fig. 6B). No significant difference could be observed in the flexibility of the MHC residues upon peptide mutation. Glu154 showed a higher flexibility in the A2/LLW-7I complex compared to the WT pMHC. However, this residue was not in contact with the mutation site, and the difference in the RMSF was not statistically significant. The only exception is the higher flexibility of

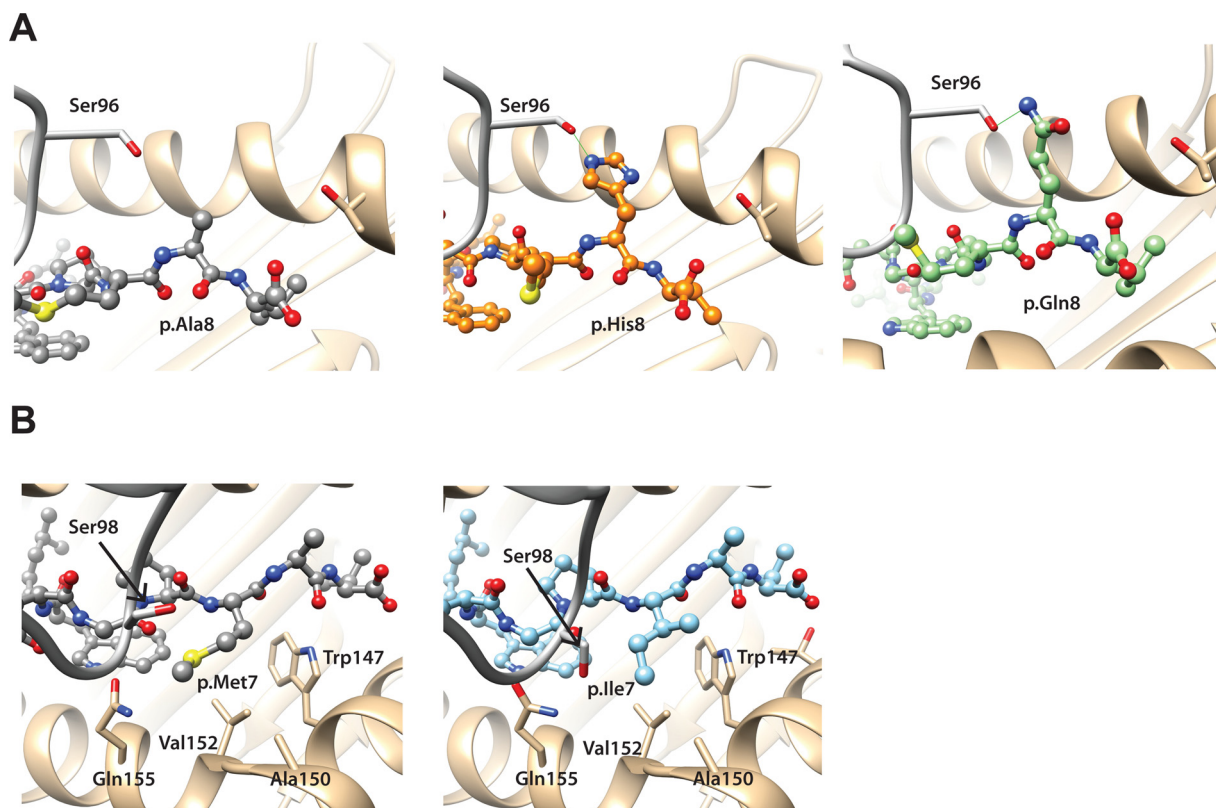


Fig. 4. Molecular modeling of the YF5048 TCR bound to the various mutant peptides in complex with HLA-A2. Ribbons represent TCR β -chain in grey; the MHC molecule in tan ribbon, and peptides in ball and stick representation. A, WT peptide on left (in grey), 8H peptide on the right (in orange), and 8Q peptide on the right (in green). C, WT peptide on left (in grey) and 7I peptide on the right (in light blue).

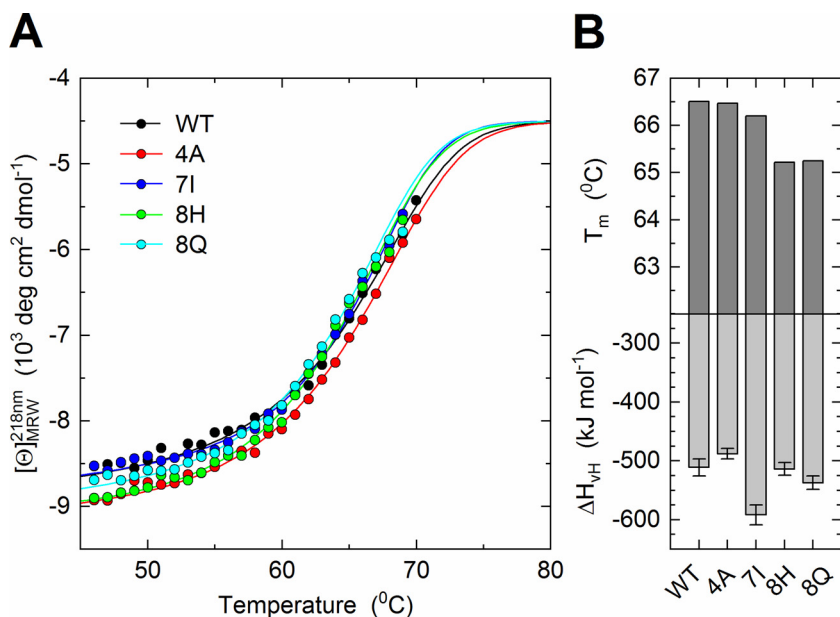


Fig. 5. Stability of the mutant peptides binding to HLA-A*0201. A) CD melting curves were recorded at 216 nm from 4 °C to circa 70 °C in a 0.1-cm cuvette at $c_{\text{prot}} \sim 3.5 \mu\text{M}$. Dots represent measured values fitted assuming a two-state trimer-to-monomer transition (solid lines). B) Apparent melting temperatures T_m (top) and van't Hoff's enthalpies of unfolding ΔH_{vH} (bottom) resulting from the fit are shown as histograms. Errors bars represent S.D. resulting from the multivariable curve fitting. Data for LLW-WT and LLW-4A were previously published (Bovay et al., 2017) and included to allow for a direct comparison.

Thr73, in the A2/LLW-7I and -8H complexes, which was statistically significant. This MHC residue is close to residues 7 and 8 of the peptide, providing a potential explanation for how its flexibility could be impacted by mutations at these positions of the peptide. However, the absolute values and the differences in the RMSF remained small.

4. Discussion

While several reports have positively correlated functional avidity

specifically to longer TCR:pMHC off-rates (Allard et al., 2017; Gannon et al., 2015; Hebeisen et al., 2015; Nauwerth et al., 2013; Schmid, 2010)), our data shows that a substitution to an isoleucine at P7 does not change the TCR:pMHC off-rates. This was further supported by our *in silico* model which shows that the 7I mutant and wild type peptides make similar interactions with the TCR. The superior T cell function induced by the LLW-7I mutant peptide is therefore not due to an increased interface with the TCR. In contrast, the LLW-8H and -8Q mutant peptides display longer TCR:pMHC off-rates and the *in silico*

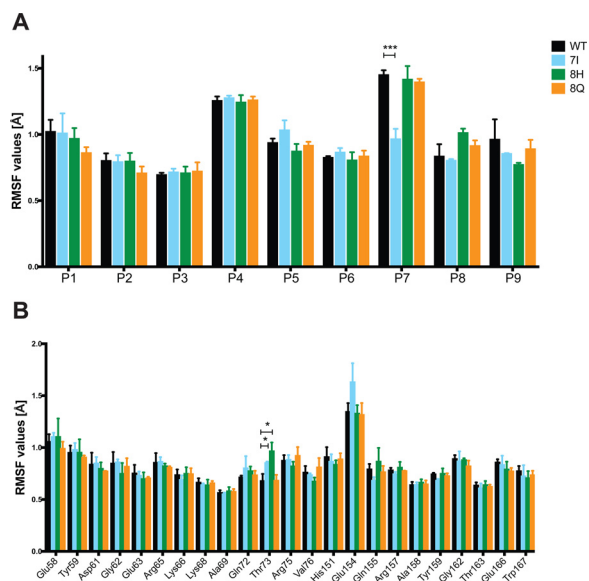


Fig. 6. Flexibility of the peptide and MHC residues. Root Mean Square Fluctuations (RMSF in Å) calculated for the peptide (A) and MHC (B) residues, averaged over 3 independent MD simulations of the LLW-WT, -7I, -8H and -8Q complexes, each 140 ns in length. Standard deviations are reported. Of note, the MD simulations were performed for the pMHC complex, in absence of the TCR. P-values from unpaired t-tests: ns = not significant, * < 0.05, ** < 0.01, *** < 0.001.

modeling suggests these peptides make more favorable contacts with the TCR, supporting the significantly higher TCR avidity compared to the WT peptide.

Position 7 of a nonamer peptide is not usually considered as a primary MHC anchor residue. We indeed did not find any significant change in thermal stability for A2/LLW-7I compared to the WT complex. However, supported by experimental ΔH_{vH} values and *in silico* molecular dynamics simulations, our results suggest that the LLW-7I mutant peptide binds the MHC molecule with higher rigidity. It has been shown that peptide motion, which also impacts MHC motion, affects recognition by the TCR (Ayres et al., 2017). Along these lines, the larger binding avidity of the A2/LLW-7I complex for the TCR compared to the A2/LLW-WT complex can be explained by the more limited flexibility of the isoleucine side chain before binding the TCR (i.e. in absence of the TCR) which translates into a lower entropy penalty upon TCR binding (Ayres et al., 2017). The A2/LLW-7I complex seems to be enthalpically favorable and more rigid than the A2/LLW-WT complex. This is supporting a better recognition of the interface by the TCR as less induced fit is required. While our experimental data shows that the 7I mutation does not alter the TCR dissociation rate (k_{off}) measured using the NTamer technology, we hypothesize it improves the TCR association rate (k_{on}) of the TCR-pMHC complex as the dissociation constant K_D (k_{on}/k_{off}) is lower than for the WT pMHC complex. Consequently, this improved K_D value could explain the 10-fold higher antigen sensitivity observed with immunoassays on the YF5048 clone.

The CPL also identified two substitutions at position 8 (LLW-8H and LLW-8Q) which behave similarly. These two substitutions showed none (LLW-8Q) or only modest (LLW-8H) enhancement of the antigen sensitivity compared to LLW-WT. However, we found that the TCR dissociation rate (k_{off} measured by NTamer) and K_D value were significantly lower compared to A2/LLW-WT. This was further supported by our *in silico* modeling suggesting that the TCR makes favorable interactions with the mutated residues. A potential explanation would be that, although 8H and 8Q substitutions improve the favorable interaction with the TCR, the threshold for maximal T cell responses might have been reached (Dutoit et al., 2001; Gannon et al., 2015; Speiser et al., 2008; Tan et al., 2015; Zhong et al., 2013).

In conclusion, our work exemplifies that the superior sensitivity of an altered peptide (LLW-7I) is not provided by an optimal interaction with the TCR. Instead, our data suggests that the improved T cell function could rather result from increased pMHC complex rigidity. This would facilitate binding to the TCR by limiting the entropy penalty, and consequently increasing the association rate as shown by an improved K_D value.

Authors contributions

AB: conceptualization, data collection, analysis and interpretation, manuscript writing. VZ: data collection, analysis and interpretation, manuscript writing. PJK: data analysis. KB: data collection, analysis and interpretation. PD: data collection. DES, DKC & SAFM: conceptualization, data interpretation, manuscript writing. All authors reviewed and approved the final version of the manuscript.

CRedit authorship contribution statement

Amandine Bovay: Conceptualization, Data curation, Formal analysis, Writing - original draft. **Vincent Zoete:** Formal analysis, Writing - original draft. **Pierre J. Rizkallah:** Formal analysis, Writing - review & editing. **Konrad Beck:** Data curation, Formal analysis, Writing - review & editing. **Philippe Delbreil:** Data curation, Writing - review & editing. **Daniel E. Speiser:** Conceptualization, Project administration, Funding acquisition, Writing - original draft. **David K. Cole:** Conceptualization, Project administration, Writing - review & editing. **Silvia A. Fuertes Marraco:** Conceptualization, Project administration, Formal analysis, Writing - original draft.

Declaration of Competing Interest

The authors declare no commercial or financial conflict of interest.

Acknowledgements

We thank staff at Diamond Light Source and at the Flow Cytometry Facility of LICR@UNIL for providing facilities and support, and Anna Fuller for the pMHC crystal plates screening and technical help. We thank the Protein Modeling Facility of Lausanne for the support in Molecular Modeling, and Dr. Michel Cuendet for providing MD simulations input files.

This project was supported by the Ludwig Cancer Research and the Cancer Research Institute (both N.Y., U.S.A), Alfred and Annemarie von Sick (Switzerland), the Swiss Cancer League (Switzerland) (3971-08-2016) and the Swiss National Science Foundation (Switzerland) grants 320030_152856 and 310030-179459.

The funders had no role in study design, data collection and interpretation, decision to submit the work for publication, or preparation of the manuscript.

Appendix A. Supplementary data

Supplementary material related to this article can be found, in the online version, at doi:<https://doi.org/10.1016/j.molimm.2020.06.025>.

References

- Abraham, Mark James, et al., 2015. GROMACS: high performance molecular simulations through multi-level parallelism from laptops to supercomputers. *SoftwareX* 1–2, 19–25.
- Akondy, Rama S., et al., 2009. The yellow fever virus vaccine induces a broad and polyfunctional human memory CD8+ t cell response. *J. Immunol.* 12 (2009), 7919–7930.
- Allard, Mathilde, et al., 2017. TCR-ligand dissociation rate is a robust and stable biomarker of CD8+ t cell potency. *JCI Insight* 14 (2017), e92570.
- Ayres, Cory M., Corcelli, Steven A., Baker, Brian M., 2017. Peptide and peptide-dependent

- motions in MHC proteins: immunological implications and biophysical underpinnings. *Front. Immunol.* 8 (2017), 935.
- Bjellmar, Pär, et al., 2010. Implementation of the CHARMM Force field in GROMACS: analysis of protein stability effects from correction maps, virtual interaction sites, and water models. *J. Chem. Theory Comput.* 2 (2010), 459–466.
- Blom, Kim, et al., 2013. Temporal dynamics of the primary human t cell response to yellow fever virus 17D as it matures from an effector- to a memory-type response. *J. Immunol.* 5 (2013), 2150–2158.
- Bovay, Amandine, et al., 2017. T cell receptor alpha variable 12-2 Bias in the immunodominant response to yellow fever virus. *Eur. J. Immunol.* (2017), 1–15.
- Bussi, Giovanni, Donadio, Davide, Parrinello, Michele, 2007. Canonical sampling through velocity rescaling. *J. Chem. Phys.* 126 (2007), 14101.
- Cole, David K., et al., 2007. Human TCR-Binding affinity is governed by MHC class restriction. *J. Immunol.* 178 (2007) 5727 LP-5734.
- Cole, David K., Yuan, Fang, Pierre, J., et al., 2009. Germ line-governed recognition of a Cancer epitope by an immunodominant human T-cell receptor. *J. Biol. Chem.* 284 (2009), 27281–27289.
- Davis, Mark M., et al., 1998. Ligand recognition by $\alpha\beta$ t cell receptors. *Annu. Rev. Immunol.* 16 (1998), 523–544.
- de Melo, Andréa Barbosa, et al., 2013. T-cell memory responses elicited by yellow fever vaccine are targeted to overlapping epitopes containing multiple HLA-I and -II binding motifs. *PLoS Negl. Trop. Dis.* 7 (2013).
- Dunbrack, Roland L., 2002. Rotamer libraries in the 21st century. *Curr. Opin. Struct. Biol.* 12 (2002), 431–440.
- Dutoit, Valérie, et al., 2001. Heterogeneous T-Cell Response to MAGE-A10(254–262):high avidity-specific cytolytic T lymphocytes show superior antitumor activity. *Cancer Res.* 61 (2001) 5850 LP-5856.
- Edgar, Robert C., 2004. MUSCLE: multiple sequence alignment with high accuracy and high throughput. *Nucleic Acids Res.* 32 (2004), 1792–1797.
- Ekeruche-Makinde, Julia, et al., 2013. Peptide length determines the outcome of TCR/peptide-MHCI engagement. *Blood* 121 (2013), 1112–1123.
- Essmann, Ulrich, et al., 1995. A smooth particle Mesh Ewald method. *J. Chem. Phys.* 103 (1995), 8577–8593.
- Eswar, Narayanan, et al., 2001. Comparative protein structure modeling using modeller. *Curr. Protoc. Bioinformatics Chapter 5: Unit-5.6.*
- Fuller, Anna, et al., 2017. Thermal stability of heterotrimeric pMHC proteins as determined by circular dichroism spectroscopy. *Bioprotocol* 7 (2017).
- Galloway, Sarah A.E., et al., 2019. Peptide super-agonist enhances T-Cell responses to melanoma. *Front. Immunol.* 10 (2019), 319.
- Gannon, Philippe O., et al., 2015. Quantitative TCR:pMHC dissociation rate assessment by NTAmers reveals antimelanoma t cell repertoires enriched for high functional competence. *J. Immunol.* 195 (2015), 356–366.
- Hebeisen, Michael, et al., 2015. Identification of rare high-avidity, tumor-reactive CD8 + T cells by monomeric TCR-ligand off-rates measurements on living cells. *Cancer Res.* 75 (2015), 1983–1991.
- Hess, Berk, Kutzner, Carsten, van der Spoel, David, Lindahl, Erik, 2008. GROMACS 4: algorithms for highly efficient, load-balanced, and scalable molecular simulation. *J. Chem. Theory Comput.* 4 (2008), 435–447.
- Holler, P.D., et al., 2001. CD8(-) t cell transfectants that express a high affinity t cell receptor exhibit enhanced peptide-dependent activation. *J. Exp. Med.* 194 (2001), 1043–1052.
- La Gruta, Nicole L., Doherty, Peter C., Turner, Stephen J., 2006. A correlation between function and selected measures of t cell avidity in influenza virus-specific CD8 + t cell responses. *Eur. J. Immunol.* 36 (2006), 2951–2959.
- MacKerell, A.D., et al., 1998. All-atom empirical potential for molecular modeling and dynamics studies of proteins. *J. Phys. Chem.* 102 (1998), 3586–3616.
- MacLachlan, Bruce J., et al., 2017. Using x-ray crystallography, biophysics, and functional assays to determine the mechanisms governing T-Cell receptor recognition of cancer antigens. *J. Vis. Exp.* 120 (2017), 54991.
- Madura, Florian, et al., 2015. Structural basis for ineffective T-Cell responses to MHC anchor residue-improved ‘heteroclitic’ peptides. *Eur. J. Immunol.* 45 (2015), 584–591.
- Marraco, Silvia A.Fuertes, et al., 2015. Long-lasting stem cell – like memory CD8 + t cells with a naive-like profile upon yellow fever vaccination. *Sci. Transl. Med.* 7 (2015).
- Matsui, K., et al., 1994. Kinetics of T-Cell receptor binding to peptide/I-Ek complexes: correlation of the dissociation rate with T-Cell responsiveness. *Proc. Natl. Acad. Sci. U.S.A.* 91 (1994), 12862–12866.
- Motozono, Chihiro, et al., 2015. Distortion of the major histocompatibility complex class I binding groove to accommodate an insulin-derived 10-Mer peptide. *J. Biol. Chem.* 290 (2015), 18924–18933.
- Nauerth, Magdalena, et al., 2013. TCR-ligand koff rate correlates with the protective capacity of antigen-specific CD8 + t cells for adoptive transfer. *Sci. Transl. Med.* 5 (2013), 192ra87.
- Petersen, Eric F., et al., 2004. UCSF chimera—a visualization system for exploratory research and analysis. *J. Comput. Chem.* 25 (2004), 1605–1612.
- Šali, Andrej, Blundell, Tom L., 1993. Comparative protein modelling by satisfaction of spatial restraints. *J. Mol. Biol.* 234 (1993), 779–815.
- Schmid, Daphné A., et al., 2010. Evidence for a TCR affinity threshold delimiting maximal CD8 t cell function. *J. Immunol.* 184 (2010) 4936 LP-4946.
- Schmidt, Julien, et al., 2011. Reversible major histocompatibility complex I-Peptide multimers containing Ni²⁺-Nitrilotriacetic acid peptides and histidine tags improve analysis and sorting of CD8 + t cells. *J. Biol. Chem.* 286 (2011) 41723–35.
- Schmidt, Julien, Dojcinovic, Danijel, Guillaume, Philippe, Luescher, Immanuel, 2013. Analysis, isolation, and activation of antigen-specific CD4 + and CD8 + T cells by soluble MHC-peptide complexes. *Front. Immunol.* 4 (2013), 1–14.
- Speiser, Daniel E., et al., 2008. Unmodified self antigen triggers human CD8 T cells with stronger tumor reactivity than altered antigen. *Proc. Natl. Acad. Sci. U.S.A.* 105 (2008), 3849–3854.
- Stone, Jennifer D., Kranz, David M., 2013. Role of t cell receptor affinity in the efficacy and specificity of adoptive t cell therapies. *Front. Immunol.* 4 (2013), 244.
- Tan, M.P., et al., 2015. T cell receptor binding affinity governs the functional profile of cancer-specific CD8 + t cells. *Clin. Exp. Immunol.* 180 (2015), 255–270.
- Tian, Shaomin, Maile, Robert, Collins, Edward J., Frelinger, Jeffrey A., 2007. CD8 + T cell activation is governed by TCR-Peptide/MHC affinity, not dissociation rate. *J. Immunol.* 179 (2007) 2952 LP-2960.
- Wooldridge, Linda, et al., 2009. Tricks with tetramers: how to get the most from multimeric peptide–MHC. *Immunology* 126 (2009), 147–164.
- Wooldridge, Linda, et al., 2012. A single autoimmune t cell receptor recognizes more than a million different peptides. *J. Biol. Chem.* 287 (2012), 1168–1177.
- Zhong, Shi, et al., 2013. T-cell receptor affinity and avidity defines antitumor response and autoimmunity in T-Cell immunotherapy. *Proc. Natl. Acad. Sci.* 110 (2013), 6973–6978.